



A flexible two-stage approach for blending multiple satellite precipitation estimates and rain gauge observations: an experiment in the northeastern Tibetan Plateau

Yingzhao Ma¹, Xun Sun^{2,3}, Haonan Chen⁴, Yang Hong⁵, Yinsheng Zhang^{6,7}

5 ¹Colorado State University, Fort Collins, CO 80523, USA

²Key Laboratory of Geographic Information Science (Ministry of Education), East China Normal University, Shanghai 200241, China

³Columbia Water Center, Earth Institute, Columbia University, New York, NY 10027, USA

⁴NOAA/Earth System Research Laboratory, Boulder, CO 80305, USA

10 ⁵School of Civil Engineering and Environmental Science, University of Oklahoma, Norman, OK 73019, USA

⁶Key Laboratory of Tibetan Environment Changes and Land Surface Processes, Institute of Tibetan Plateau Research, Chinese Academy of Sciences, Beijing, 100101, China

⁷CAS Center for Excellence in Tibetan Plateau Earth Sciences, Beijing, 100101, China

Correspondence to: Xun Sun (xs2226@columbia.edu)

15 **Abstract.** Substantial biases exist in the Satellite Precipitation Estimates (SPE) over complex terrain regions and it has always been a challenge to quantify and correct such biases. The combination of multiple SPE and ground observations would be beneficial to improve the precipitation estimates. In this study, a flexible two-step approach is proposed by firstly reducing the systematic errors of each SPE using rain gauge observations as references, and then merging the improved multi-SPE with a Bayesian weighting model. In the 1st stage, gauge references are assumed as a generalized regression function of SPE and terrain feature. In the 2nd stage, the weights assigned to the involved SPE are calculated according to the associated performance relative to gauge references. This blending method has the ability to exert benefits from multi-SPE in terms of higher performance and mitigate negative impacts from the ones with lower quality. In addition, Bayesian analysis is applied in the two phases by specifying prior distributions on the model parameters, which enables to produce posterior ensembles associated with their predictive uncertainties. The performance of the two-step blending approach is assessed using independent rain gauge observations during the warm season of 2014 in the northeastern Tibetan Plateau. Results show that the blended multi-SPE are significantly improved compared to the original individuals, especially during heavy rainfall events. This study can also be expanded as a data fusion framework in the development of high-quality precipitation products in high-cold regions characterized by complex terrain.

20
25

1 Introduction

30 High-quality precipitation data is fundamental to understand the regional and global hydrological processes. However, it is still difficult to acquire accurate precipitation information in the mountainous regions, e.g., Tibetan Plateau (TP), due to limited



ground sensors (Ma et al., 2015). The satellite sensors are capable of providing precipitation estimates at a large scale (Hou et al., 2014), but performances of available satellite products vary among different retrieval methods and climatic areas (Yong et al., 2015; Prat and Nelson, 2015; Ma et al., 2016). Thus, it is suggested to incorporate precipitation estimates from multiple
35 sources into a fusion procedure with fully consideration of the strength of individual members and associated uncertainty.

Precipitation data fusion was initially reported by merging radar-gauge rainfall in the mid-1980s (Krajewski, 1987). The Global Precipitation Climatology Project (GPCP) was an earlier attempt for satellite-gauge data fusion, which adopted a mean bias-corrected method and an inverse-error-variance weighting approach to develop a monthly, 0.25° global precipitation data
40 (Huffman et al., 1997). Another popular dataset, Climate Prediction Center Merged Analysis of Precipitation (CMAP), included global monthly precipitation with a 2.5° x 2.5° resolution for a 17-year period by merging gauges, satellites and reanalysis data using the maximum likelihood estimation method (Xie and Arkin, 1997). Since then, several blending approaches have been developed to generate rainfall products with higher quality by merging gauge, radar and satellite observations (e.g., Li et al., 2015; Beck et al., 2017; Xie and Xiong, 2011; Yang et al., 2017; Baez-Villanueva et al., 2020).
45 Overall, those fusion methods follow a general concept by eliminating biases in satellite/radar-based data and then merging the bias-adjusted satellite/radar estimates with point-wise gauge observations. However, these efforts might be insufficient for quantifying the predicted data uncertainty. Some blended estimates are also partially polluted by the poorly performed individuals (Tang et al., 2018). Therefore, this paper develops a new blending algorithm that enhances the quantitative modeling of individual error structures, prevents potential negative impacts from lower-quality members, and enables an
50 explicit description of the model's predictive uncertainty. In addition, a Bayesian concept for accurate rainfall estimates is proposed based on these conditions. The Bayesian analysis has the advantage of a statistically post-processing idea that could yield a predictive distribution with quantitative uncertainty (Renard, 2011). For instance, a Bayesian kriging approach, which assumes a Gaussian process for precipitation at any location and considers the elevation as a covariate, is developed for merging monthly satellite and gauge precipitation data (Verdin et al., 2015). A dynamic Bayesian model averaging method is
55 applied for satellite precipitation data merging across the TP (Ma et al., 2018). Given the flexible distribution of multiple sources of precipitation biases in regions with complex terrain, continuous efforts should be taken to exert the potential merit of Bayesian approach on this critical issue.

In this paper, a two-step approach is described for blending multiple Satellite Precipitation Estimates (multi-SPE) and point-
60 based rain gauge observations. The initial experiment is performed during the warm season of 2014 in the northeastern TP (NETP), where a denser network of rain gauges is available compared to other regions of TP. The proposed two-stage blending approach is also expected to help with the exploration of multi-source/scale precipitation data merging in other regions with complex terrain.



65 The paper is organized as follows: Section 2 gives a brief introduction of the study area and precipitation data sources. Section 3 details the proposed two-stage blending approach. Results and discussions are presented in Sections 4 and 5, respectively. The primary summary and future work are provided in Section 6.

2 Study area and dataset

70 The selected study domain is located in the upper Yellow River basin of northeastern TP (Fig. 1). As shown in the 90-m digital elevation data, the elevation ranges from 785 m in the northeast to 6252 m in the southeast. The total annual precipitation is around 500 mm and the mean annual air temperature is 0.7°C (Cuo et al., 2013). To avoid snowfall contamination in the cold season, the warm period from May 1st, to September 30th in 2014 is selected in this demonstration study.

Four popular SPE are used, including Precipitation Estimation from Remotely Sensed Information using Artificial Neural Networks (PERSIANN) - Climate Data Records (PERCDR) (Ashouri et al., 2015), Tropical Rainfall Measuring Mission (TRMM) Multi-satellite Precipitation Analysis 3B42 Version 7 (3B42V7) (Huffman et al., 2007), Climate Prediction Center (CPC) Morphing technique for the bias-corrected product (CMORPH) (Joyce et al., 2004), and the Integrated Multi-satellitE Retrievals for the Global Precipitation Measurement (GPM) mission (IMERG) (Huffman et al., 2018) (Table 1). Since IMERG data has a spatial resolution of $0.10^{\circ} \times 0.10^{\circ}$, and other SPE (i.e., PERCDR, 3B42V7 and CMORPH) have a spatial resolution
80 of $0.25^{\circ} \times 0.25^{\circ}$. The IMERG data are resampled from 0.10° to 0.25° so as to match the other individuals before performing the two-stage blending.

A ground rain gauge network including 34 stations are used in this study (Fig. 1). The gauge data are carefully checked to ensure its creditability (Shen and Xiong, 2016). All of them are independent from the Global Precipitation Climatology Center (GPCC) stations, which are used for bias adjustment of the TRMM/GPM-era data, such as 3B42V7 and IMERG (Huffman et al., 2007; Hou et al., 2014). In addition, the gauge network is randomly classified into two parts: the black dots are used for training the model, and the remaining ones are for model verification. In order to demonstrate the reliability of the proposed two-stage blending approach, the selection of training sites is randomly repeated for 10 times to further examine the blending performance. In addition, the proposed blending algorithm is applied on a heavy rainfall case of Sep 22, 2014 in the NETP, to
90 quantify the performance during heavy rainfall scenario. Local recycling performs as a premier role for the moisture sources of rainfall extremes in the NETP (Ma et al., 2020). This case is a typical storm that could stand for the local heavy rainfall patterns to a large extent during the warm season.



3 A two-stage blending algorithm

3.1 Overview

95 This algorithm aims at developing a multi-source data merging framework so as to provide the best-available precipitation
product in any region of interest. Let $R(s, t)$ denote near-surface precipitation at gauge site s and the t^{th} day in a year. The
original and bias-adjusted multi-SPE at the same location and time are defined as $(Y_1(s, t), Y_2(s, t), \dots, Y_p(s, t))$ and
 $(Y'_1(s, t), Y'_2(s, t), \dots, Y'_p(s, t))$, respectively. For simplicity, they are accordingly replaced by R , (Y_1, Y_2, \dots, Y_p) , and
 $(Y'_1, Y'_2, \dots, Y'_p)$. Noted that the value of p equals to 4 in this study, where PERCDR, 3B42V7, CMORPH and IMERG refers to
100 Y_1, Y_2, Y_3, Y_4 , respectively.

The diagram of the proposed two-stage blending approach is shown in Figure 2. Stage 1 is designed to correct the systematic
errors of individual SPE using point-based rain gauge observations (training sites) as ground references, where the assumptions
of various probabilistic distribution for gauge references conditional on each SPE are not limited to Gaussian prototype. The
105 impact of topography is also considered. In the 2nd step, a Bayesian weight model is applied to blend the improved multi-SPE.
It has the ability to exert benefits from multi-SPE of higher performance and mitigate negative impacts from the ones with
lower quality. It is expected to produce posterior blended results associated with their predictive uncertainties in the survey
region.

110 The details of the two-stage blending algorithm are described in Sections 3.2 and 3.3, respectively.

3.2 Stage 1: Bias adjustment

A generalized regression function between gauge references, individual SPE, and terrain features is proposed in the 1st stage.
Because the bias of SPE generally follows a skew Normal distribution, it is important to fit an appropriate function. In this
paper, a Student's t distribution is assumed for modelling of gauge observations conditional on the individual SPE. It is written
115 as:

$$R|Y_i \sim Student(\nu_i, \alpha_i + \beta_i * Y_i + \gamma_i * Z, \sigma_i), \alpha_i, \beta_i, \gamma_i \in R, \nu_i, \sigma_i \in R^+ \quad (1)$$

where $\theta = \{\nu_i, \alpha_i, \beta_i, \gamma_i, \sigma_i\}$ are model parameter sets in order to adjust the i^{th} SPE. $(\alpha_i + \beta_i * Y_i + \gamma_i * Z)$ represents the
sample mean and Z is the associated collection of covariates (e.g., topography). More specifically, the normalized elevation is
used as a covariate in this experiment. These parameters are real numbers and ν_i, σ_i are positive. It should be noted that some
120 other distributions (e.g., Lognormal, Normal) are also examined but there are no obvious improvements in terms of the bias-
adjusted result compared to Student's t distribution for this test.

Based on the gauge observations and multi-SPE at the training sites, model parameters for each SPE could be estimated within
a Bayesian analysis using the Markov Chain Monte Carlo (MCMC) technique (Gelman et al., 2013). Next, it is to calculate



125 each of the bias-adjusted SPE at any new site (s') of the domain at the same period. The conditional distribution of bias-
adjusted SPE at any new site is mathematically defined as:

$$f(R_{s'}|Y_i) = \int f(R_{s'}, \boldsymbol{\theta}|Y_i) d\boldsymbol{\theta} \quad (2a)$$

$$= \int f(R_{s'}|\boldsymbol{\theta})f(\boldsymbol{\theta}|Y_i) d\boldsymbol{\theta} \quad (2b)$$

where the posterior distribution of $R_{s'}|Y_i$ from Eq. 2 can be simulated numerically based on the calculated parameter samples
130 $\boldsymbol{\theta}$ at the training sites using the MCMC samplings. We further assume N as the size of post-convergence MCMC samples. The
above process is repeated N times and produces a predictive posterior distribution at any new site s' and time t .

3.3 Stage 2: Data merging

On the basis of Stage 1, this part is designed to blend the updated multi-SPE at each grid cell of the domain. With regard to
the individual SPE, the median value of the posterior samples from Stage 1 is assumed as the new SPE. Here, we redefine the
135 bias-adjusted multi-SPE as $Y'_i (i = 1, 2, \dots, p)$, respectively.

The formulas of blending the bias-adjusted multi-SPE are shown below:

$$B = \sum_{i=1}^p Y'_i * w_i + \varepsilon, w_i \in R(0,1), \varepsilon \in R^+ \quad (3)$$

$$\sum_{i=1}^p w_i = 1 \quad (4)$$

140 where B means the blended result; $w_i (i=1, 2, \dots, p)$ stands for the relative weight of the i^{th} SPE, respectively, and their values
range from 0 to 1; ε is the residual error, whose value is positive real number. Ideally, the blended multi-SPE, i.e., B , at the
training site s and time t should be close to gauge references $R(s, t)$. Thereby, the weight parameters, including $w_i (i = 1, 2, \dots, p)$
and ε are able to be estimated at the training sites based on gauge observations and new multi-SPE within a Bayesian analysis
using the MCMC technique.

145

As the weight parameters are successfully derived above, similar to Eq. 4, the blended result at any new sites at time t are
calculated based on the retrieved new multi-SPE and corresponding optimal weights. Finally, we can obtain spatial patterns of
blended multi-SPE and point-based rain gauge observations in terms of the median, standard deviation (SD) and associated
confidence intervals (e.g., 5% and 95% quantiles) in regions of interest.

150 4 Results

To assess the performance of the proposed two-stage blending method, several statistical error indices including Root Mean
Square Errors (RMSE), Normalized Mean Absolute Errors (NMAE), and the Pearson's Correlation Coefficients (CC) are used
in this study. The specific formulas of these metrics can be found in Chen et al. (2019).



4.1 Bias adjustment of multi-SPE

155 Compared to the gauge references, the original multi-SPE including PERCDR, 3B42V7, CMORPH and IMERG show significant biases at the independent validation sites over the NETP during the warm season of 2014 (Table 2). Their statistical error metrics range from 6.59-8.07 mm/d, 63.2-83.5%, and 0.40-0.57, in terms of RMSE, NMAE, and CC, respectively. 3B42V7 performs the worst with the highest RMSE and NMAE at 8.07 mm/d and 83.5%, and the lowest CC of 0.40. IMERG shows the best performance in terms of the lowest NMAE at 63.2% and highest CC at 0.57 among the four SPE. It seems that
160 the satellite retrievals need to be further clarified with regard to the mainstream SPE in the NETP.

After the bias adjustment of each SPE, the updated multi-SPE show great improvement in data quality during this experiment (Fig. 3). These changes result in better agreement of SPE with rain gauge measurements at the validated sites in the NETP. Both RMSE and NMAE of the corrected multi-SPE are correspondingly decreasing in terms of 4.56~5.06 mm/d and
165 50.9~58.7%, respectively. As compared with the original multi-SPE, the updated ones decrease by 27~37.3% and 19.1~31.1% with respect to RMSE and NMAE, respectively. Moreover, the CC index of four SPE vary from 0.42 to 0.57 after bias adjustment, which slightly increases as compared to the original SPE. It is also found that 3B42V7 improves the most in terms of its RMSE decreasing from 8.07 mm to 5.06 mm using the step 1's method. Basically, it implies that the proposed bias-adjusted algorithm occurred in phase 1 is very effective for reducing systematic errors of four involved SPE in the warm season
170 of 2014 in the NETP.

4.2 Blending multi-SPE and independent validation

To test the performance of the proposed two-step blending approach, the blended multi-SPE at the validation sites are further examined. As shown in Figure 3, the fusion result is closer to the ground reference in terms of RMSE, NMAE and CC, compared to the individual SPE. The RMSE and NMAE indices of the merging data decrease by 34.1~65.4% and 27.1~41.1%,
175 respectively, compared to the individual SPE, while the CC index increases by 6.7~50.4%, accordingly (Table 2). Compared to the bias-corrected multi-SPE, the performance of the blended data increases by 5.1~14.2%, 3.3~16.2%, and 5.9~47.8% in terms of RMSE, NMAE and CC, respectively. That is to say, the merged precipitation in the warm season of 2014 at the validated sites of NETP exhibit higher quality after merging the bias-corrected multi-SPE using the optimal relative weights shown in Figure 4a. The blended data have been effectively dropped towards the gauge references at the validation sites, which
180 is evidenced from the scatterplots in terms of red dots in Figure 4b. These improvements prove the significant superiority of the two-step blending method on reducing the systematic errors of the original multi-SPE and supplying higher daily precipitation in the warm season of 2014 over the NETP.

The best-performed merging result is due to the ensemble contributions of the bias-corrected multi-SPE. The optimally relative
185 weights are 0.019, 0.052, 0.289, and 0.640 with respect to PERCDR, 3B42V7, CMORPH and IMERG, respectively. It shows



that the bias-adjusted IMERG and PERCDR contributes the highest and lowest weights, respectively, in this blending process, and the contributions of the other SPE rank between IMERG and PERCDR accordingly. As the bias-adjusted IMERG shows the best performance among all the individuals, it proves that higher informative SPE shows more positive impact on the blended result under this two-step fusion approach. It is further concluded that this blending method has its ability to exert
190 benefits from multi-SPE in terms of higher performance and mitigate poor impacts from the ones with lower quality.

4.3 Model clarification with random verified sites

Figure 5 shows the evaluation scores of RMSE, NMAE, and CC for the original multi-SPE and blended estimates at the validation sites with 10 random split of the gauge stations. For each test, 7 gauge sites are randomly selected from the 34 sites and used for model verification, and the remaining 27 gauge sites are used for model fitting.

195

As for the blended result, it performs similar skill scores at the independent sites for the 10 random tests. It also shows better performance in terms of RMSE, NMAE and CC, which are 4.34~5.57 mm/h, 49.2~61.7%, and 0.49~0.67, respectively, compared to the raw multi-SPE at each random experiment. Statistically, the averaged values of RMSE, NMAE and CC for the blended data at the validation sites are 4.98 mm/h, 54.9% and 0.60, respectively, while the four SPE range from 6.21~7.72
200 mm/d, 66.3~78.9%, and 0.38~0.57, respectively (Table 3). The averaged improvement ratios of RMSE for the blended data are 35.1%, 33.7%, 19.6% and 32.1% compared to PERCDR, 3B42V7, CMORPH and IMERG, respectively (Table 4). Similar performance is seen from the NMAE scores, where their mean improvement ratios are 29.8%, 30.1%, 17.0% and 21.3%, respectively for the four SPE. As seen in Figure 6, the blended result shows a significant improvement over the original multi-SPE in the survey area, especially for PERCDR and 3B42V7. It is concluded that the biases of multi-SPE could be significantly
205 reduced as the impacts of bias functions are well considered in the proposed two-step blending algorithm.

4.4 Model application in spatial domain

It is important to explore the Bayesian ensembles at any unknown sites in the study domain. Therefore, the two-step blending approach is applied on the four spatially distributed SPE (i.e., PERCDR, 3B42V7, CMORPH, IMERG) from Figures 7a to 7d to obtain blended estimates of daily mean precipitation in the warm season of 2014 for the whole study domain (not only at
210 the gauge stations). Spatial maps of the merging predictions and the associated predictive uncertainties including SD, 5% and 95% quantiles are shown along with the gauge observations (Figure 8).

All of the multi-SPE have the ability in capturing the spatial patterns of daily mean precipitation during the warm season, but might fail in the representation of precipitation amounts in the NETP (Figure 7), likely because of the satellite retrieval biases
215 in complex terrain and limited ground validation network. The spatial patterns of blended multi-SPE are shown in Figure 8a, which has a similar spatial pattern with a higher precipitation amounts in the southwest compared with the individual SPE. Based on the proposed blending approach, the fusion estimate performs a higher adjustment compared to the original SPE. It



is expected to show a better performance in terms of magnitude and distribution in the study area. Moreover, the predictive uncertainties are displayed from Figures 8b to 8d so as to illustrate the blending variance. In total, this study confirms the priority of exploring daily precipitation in spatial at higher accuracy and quantifying the associated uncertainty in the study domain.

4.5 Model performance on a heavy rainfall case

Accurate precipitation on extreme weather is very important for flood hazard mitigation. Here, we investigate the utility of this two-step blending approach on a heavy rainfall event of Sep 22, 2014 in the NETP (Figure 9a). The relative weights of PERCDR, 3B42V7, CMORPH, and IMERG for the blended data are 0.464, 0.123, 0.112 and 0.301, respectively, during this particular heavy rainfall event (Figure 9b).

Table 4 reports the evaluation statistics reflecting the blended model performance on this heavy rainfall case, where the RMSE, NMAE and CC indices of the individual SPE range from 6.28~10.48 mm/d, 40.6~59.5%, and 0.69~0.82, respectively. Overall, compared to the individuals the merged product has lower RMSE and NMAE and higher CC values, which are 4.13 mm/d, 27.4%, and 0.85, respectively. In other words, the RMSE and NMAE indices of the blended result decrease by 34.2~60.6% and 32.5~53.9%, respectively, while the CC index correspondingly increases by 3.4~23.9% on this heavy rainfall case compared to the individuals. The two-step blending approach has a great influence on the performance of SPE in terms of rainfall extremes in the warm season of the NETP.

The blended model performance is further explored at three gauge sites (i.e., IDs 56171, 56152, 56182) with the top three rainfall records in terms of daily rainfall amounts on Sep 22, 2014 (Figure 9a). Figure 10 shows the Probabilistic Density Function (PDF) curves of blended samples of the above three sites during this event. It aims to demonstrate the blended performance on quantifying the predictive uncertainty on rainfall extremes in the survey region. At ID 56171, the estimated rainfall derived from PERCDR, 3B42V7, CMORPH and IMERG are 19.8 mm, 35.3 mm, 26 mm, and 40.2 mm, respectively. 3B42V7 and IMERG shows an overestimation, while PERCDR and CMORPH underperform the daily rainfall at the corresponding pixel (Figure 10a). Based on the two-step blending methods, the median and SD values of the merging estimates are 24.1 mm/d, and 4.4 mm/d, respectively. At IDs 56152 and 56182, the median/SD values of blended multi-SPE are 24.3/5.0 mm/d and 21.9/4.5 mm/d, respectively. As learned from Figures 10b and 10c, the medians of the blended result at IDs 56152 and 56182 are very close to gauge observations in terms of 24.6 mm, and 23.1 mm, respectively. It shows that this two-step fusion algorithm provides a posterior inference and quantifies its predictive uncertainties on the heavy rainfall events. It is confirmed that the proposed two-step blending method is able to improve the daily precipitation amounts even during rainfall extremes in the NETP.



5 Discussions

250 This study proposes a flexible two-step blending algorithm for merging multi-satellite and rain gauge precipitation data at daily scale, aiming to provide a more accurate precipitation datasets in regions with complex terrain. In spite of superior performance of the merging results, some issues still need to clarify:

Because of limited knowledge on the influences of complex terrain and local climate on the rainfall patterns in the study area, 255 the elevation feature is merely considered in the first stage. It is noted that deep convective systems occurring near mountainous have an effect on the precipitation cloud (Houze, 2012), which should be considered in future to resolve the impact of orography on the adjustment of individual SPE. In addition, as calculating the blended result in any new sites, the model parameters derived from the training sites are assumed to be applicable in the domain. Since the domain of this study is not very large and we have a relatively dense rain gauge network, the current assumption seems to be acceptable according to the 260 performance of the blended data. However, it is noted that, if extended to the TP or the global scale, the extension of model parameters should be carefully considered. For instance, there are few gauges installed in the western and central TP (Ma et al., 2015), it might be a potential risk to directly apply this fusion algorithm for these regions.

The goal of this study is not to model rainfall process in a target domain, but to propose an idea to extract valuable information 265 from available multi-satellite sources and provide more reliable precipitation in high-cold regions with complex topography. Considering its spatiotemporal differences and the existence of many zero-value records, rainfall is extremely difficult to observe and predict (Yong et al., 2015; Bartsotas et al., 2018). With regard to the probability of rainfall occurrence, a zero-inflated model, which is coherent with the empirical distribution of rainfall data, is expected to further improve the two-step fusion algorithm. In addition, hourly or even instantaneous precipitation intensity is extremely vital for flood prediction, which 270 should be considered when extending this framework.

6 Summary and prospects

This study proposes a two-step blending algorithm for multi-SPE data fusion. A preliminary experiment is conducted over the NETP using four mainstream SPE to demonstrate the performance of this fusion approach, including PERCDR, 3B42V7, CMORPH, and IMERG. Primary conclusions are summarized below:

275

(1) This blending algorithm is designed with high flexibility, which is capable of involving a group of multi-SPE that may follow different probabilistic distributions conditional on ground references. In addition, it provides a convenient way to compare the merging performance and further quantify the associated fusion uncertainties.



280 (2) The case studies show that the merged precipitation has higher skill scores compared with the individual SPE at the independent validation sites. The 10 random verification tests further confirms the superiority of the proposed two-step blending algorithm. The performance of this fusion algorithm is further demonstrated for the heavy rainfall event.

(3) The experiment proves that this algorithm can allocate the contribution of individual SPE on the blended prediction because
285 it is capable of ingesting useful information from uneven individuals and alleviating potential negative impacts from the poorly performing members.

Overall, this work provides an opportunity for blending multi-SPE products. It is expected to promote the development of higher quality precipitation product in the remotely high-cold regions with widely available satellite precipitation retrievals.
290 The exploration of model reliability of this two-step blending algorithm at larger scale (e.g., the TP) and higher temporal resolution (e.g., hourly) should be pursued in a future study.

Data availability

The gauge data are from China Meteorological Data Service Center (<http://data.cma.cn>). The PERCDR data are obtained from <http://www.ncei.noaa.gov/data/precipitation-persiann/>; the 3B42V7 data are obtained from <https://pmm.nasa.gov/data-access/downloads/trmm>; the CMORPH data are obtained from ftp://ftp.cpc.ncep.noaa.gov/precip/CMORPH_V1.0; the IMERG data are obtained from <https://pmm.nasa.gov/data-access/downloads/gpm>.
295

Author contributions

YM, XS and YH conceive the idea; XS, YH and YZ provide the project and financial supports. YM conduce the detailed analysis; HC, XS and YZ give comments on the analysis; all the authors contribute to the writing and revisions.

Competing interests

300

The authors declare that they have no conflict of interest.

Acknowledgements

This study is supported by the National Key Research and Development Program of China (No. 2017YFA0603101), Strategic Priority Research Program (A) of CAS (No. XDA2006020102), and the National Natural Science Foundation of China (No. 91437214). We also thank Dr. Ning Ma from the Institute of Tibetan Plateau Research, Chinese Academy of Sciences, for the
305 great comments and suggestions.



References

- Ashouri, H., Hsu, K. L., Sorooshian, S., Braithwaite, D. K., Knapp, K. R., Cecil, L. D., Nelson, B. R., and Prat O. P.:
310 PERSIANN-CDR: Daily Precipitation Climate Data Record from Multisatellite Observations for Hydrological and Climate
Studies, *Bull. Amer. Meteor. Soc.*, 96, 69-83, 2015.
- Baez-Villanueva, O. M., Zambrano-Bigiarini, M., Beck, H. E., McNamara, I., Ribbe, L., Nauditt, A., Birkel, C., Verbist, K.,
Giraldo-Osorio, J. D., and Thinh, N. X.: RF-MEP: A novel Random Forest method for merging gridded precipitation
products and ground-based measurements, *Remote Sens. Environ.*, 239, 111606, 2020.
- Bartsotas, N. S., Anagnostou, E. N., Nikolopoulos, E. I., and Kallos, G.: Investigating satellite precipitation uncertainty over
315 complex terrain, *J. Geophys. Res.-Atmos.*, 123, 5346-5369, 2018.
- Beck, H. E., van Dijk, A. I. J. M., Levizzani, V., Schellekens, J., Miralles, D. J., Martens, B., and de Roo A.: MSWEP: 3-
hourly 0.25° global gridded precipitation (1979-2015) by merging gauge, satellite, and reanalysis data, *Hydrol. Earth Syst.
Sci.*, 21, 589-615, 2017.
- Chen, H., Cifelli, R., Chandrasekar, V., and Ma, Y.: A flexible Bayesian approach to bias correction of radar-derived
320 precipitation estimates over complex terrain: model design and initial verification, *J. Hydrometeorol.*, 20, 2367-2382, 2019.
- Cuo, L., Zhang, Y., Gao, Y., Hao, Z., and Cairang L.: The impacts of climate change and land cover/use transition on the
hydrology in the upper Yellow River Basin, China, *J. Hydro.*, 502, 37-52, 2013.
- Gelman, A., Carlin, J. B., Stern, H. S., Dunson, D. B., Vehtari, A., and Rubin D. B.: *Bayesian Data Analysis-Third Edition*,
CPC Press. 2013.
- 325 Hou, A. Y., Kakar, R. K., Neeck, S., Azarbarzin, A. A., Kummerow, C. D., Kojima, M., Oki, R., Nakamura, K., and Iguchi,
T.: The Global Precipitation Measurement Mission, *Bull. Amer. Meteor. Soc.*, 95, 701-722, 2014.
- Houze., R. A.: Orographic effects on precipitating clouds, *Rev. Geophys.*, 50, RG1001, 2012.
- Huffman, G., Adler, R., Arkin, P., Chang, A., Ferraro, R., Gruber, A., Janowiak, J. E., McNab, A., Rudolf, B., and
Schneider, U.: The global precipitation climatology project (GPCP) combined precipitation dataset, *Bull. Amer. Meteor.*
330 *Soc.*, 78, 5-20, 1997.
- Huffman, G. J., Bolvin, D. T., Nelkin, E. J., Wolff, D. B., Adler, R. F., Gu, G., Hong, Y., Bowman, K. P., and Stocker E. F.:
The TRMM Multisatellite Precipitation Analysis (TMPA): quasi-global, multiyear, combined-sensor precipitation estimates
at fine scales, *J. Hydrometeorol.*, 8, 38-55, 2007.
- Huffman, G. J., Bolvin, D. T., Braithwaite, D., Hsu, K., Joyce, R., Kidd, C., Nelkin, E. J., Sorooshian, S., Tan, J., and Xie,
335 P.: NASA Global Precipitation Measurement (GPM) Integrated Multi-satellitE Retrievals for GPM (IMERG), Algorithm
Theoretical Basis Document (ATBD) Version 5.2, NASA/GSFC, Greenbelt, MD, USA, 2018.
- Joyce, R. J., Janowiak, J. E., Arkin, P. A. and Xie, P.: CMORPH: A method that produces global precipitation estimates
from passive microwave and infrared data at high spatial and temporal resolution, *J. Hydrometeorol.*, 5, 487-503, 2004.
- Krajewski, W. F.: Cokriging radar-rainfall and rain gage data, *J. Geophys. Res.*, 92, 9571-9580, 1987.



- 340 Li, H., Hong, Y., Xie, P., Gao, J., Niu, Z., Kirstetter, P. E., and Yong, B.: Variational merged of hourly gauge-satellite precipitation in China: preliminary results, *J. Geophys. Res.-Atmos.*, 120, 9897-9915, 2015.
- Ma, Y., Zhang, Y., Yang, D., and Farhan S. B.: Precipitation bias variability versus various gauges under different climatic conditions over the Third Pole Environment (TPE) region, *Int. J. Climatol.*, 35, 1201-1211, 2015.
- Ma, Y., Tang, G., Long, D., Yong, B., Zhong, L., Wan, W., and Hong, Y.: Similarity and error intercomparison of the GPM
345 and its predecessor-TRMM Multi-satellite Precipitation Analysis using the best available hourly gauge network over the Tibetan Plateau, *Remote Sensing*, 8, 569, 2016.
- Ma, Y., Hong, Y., Chen, Y., Yang, Y., Tang, G., Yao, Y., Long, D., Li, C., Han, Z., and Liu, R.: Performance of optimally merged multisatellite precipitation products using the dynamic Bayesian model averaging scheme over the Tibetan Plateau, *J. Geophys. Res.-Atmos.*, 123, 814-834, 2018.
- 350 Ma, Y., M. Lu, C. Bracken, and H. Chen.: Spatially coherent clusters of summer precipitation extremes in the Tibetan Plateau: Where is the moisture from? *Atmos. Res.*, 237, 104841, 2020.
- Prat, O. P., and Nelson, B. R.: Evaluation of precipitation estimates over CONUS derived from satellite, radar, and rain gauge data sets at daily to annual scales (2002-2012), *Hydrol. Earth Syst. Sci.*, 19, 2037-2056, 2015.
- Renard, B.: A Bayesian hierarchical approach to regional frequency analysis, *Water Resour. Res.*, 47, W11513, 2011.
- 355 Sanso, B., and Guenni, L.: Venezuelan rainfall data analysed by using a Bayesian space time model, *J. R. Stat. Soc. C.-Appl.*, 48, 345-362, 1999.
- Shen, Y., and Xiong, A.: Validation and comparison of a new gauge-based precipitation analysis over mainland China, *Int. J. Climatol.*, 36, 252-265, 2016.
- Tang, Y., Yang, X., Zhang, W., and Zhang, G.: Radar and Rain Gauge Merging-Based Precipitation Estimation via
360 Geographical-Temporal Attention Continuous Conditional Random Field, *IEEE Trans Geosci Remote Sens.*, 56, 1-14, 2018.
- Tian, Y., Huffman, G. J., Adler, R. F., Tang, L., Sapiano, M., Maggioni, V., and Wu, H.: Modeling errors in daily precipitation measurements: additive or multiplicative, *Geophys. Res. Lett.*, 40, 2060-2065, 2013.
- Verdin, A., Rajagopalan, B., Kleiber, W., and Funk, C.: A Bayesian kriging approach for blending satellite and ground precipitation observations, *Water Resour. Res.*, 51, 908-921, 2015.
- 365 Xie, P., and Arkin, P.: Global precipitation: a 17-year monthly analysis based on gauge observations, satellite estimates, and numerical model outputs, *Bull. Amer. Meteor. Soc.*, 78, 2539-2558, 1997.
- Xie, P., Xiong, A.-Y.: A conceptual model for constructing high-resolution gaugesatellite merged precipitation analyses, *J. Geophys. Res.-Atmos.* 116, D21106, 2011.
- Yang, Z., Hsu, K., Sorooshian, S., Xu, X., Braithwaite, D., Zhang, Y., and Verbist, K.M.J.: Merging high-resolution
370 satellite-based precipitation fields and point-scale rain gauge measurements - a case study in Chile, *J. Geophys. Res.-Atmos.*, 122, 5267-5284, 2017.



Yong, B., Liu, D., Gourley, J. J., Tian, Y., Huffman, G. J., Ren, L., and Hong, Y.: Global View Of Real-Time Trmm Multisatellite Precipitation Analysis: Implications For Its Successor Global Precipitation Measurement Mission, *Bull. Amer. Meteor. Soc.*, 96, 283-296, 2015.

375 **Figure and Table Captions**

Table 1: Basic information of multi-SPE used in this study.

Table 2: Summary of statistical error indices (i.e., RMSE, NMAE, and CC) in terms of the original, bias-adjusted, and blended multi-SPE (i.e., PERCDR, 3B42V7, CMORPH, and IMERG) at the validated sites of NETP in the warm season of 2014.

380 **Table 3:** Summary of the mean values of statistics including RMSE, NMAE and CC in terms of the original and blended multi-SPE (i.e., PERCDR, 3B42V7, CMORPH, and IMERG) at 10 random verified tests in the warm season of 2014 over the NETP.

Table 4: Summary of the mean improvement ratios of statistics including RMSE, NMAE and CC in terms of the blended multi-SPE as compared to the original PERCDR, 3B42V7, CMORPH, and IMERG at 10 random verified tests in the warm
385 season of 2014 over the NETP.

Table 5: Summary of statistical error indices (i.e., RMSE, NMAE, and CC) in terms of the original and blended multi-SPE (i.e., PERCDR, 3B42V7, CMORPH, and IMERG) during a heavy rainfall event over the NETP on Sep 22, 2014.

Figure 1: Overview of the topography and gauge observation network used in the study, where 27 gauges (black dots) are used for training and 7 (red dots) are used for independent verification.

390 **Figure 2:** The diagram of the proposed two-step blending algorithm.

Figure 3: Intercomparisons of statistical error indices for the original, bias-adjusted, and blended multi-SPE at the validated sites during the warm season of 2014: (a) RMSE, (b) NMAE, and (c) CC.

Figure 4: (a) The Box-Whisker plots of relative weights of the bias-adjusted multi-SPE (i.e., PERCDR, 3B42V7, CMORPH and IMERG) in the stage 2 process; (b) intercomparison of the original and blended multi-SPE at the validated sites during
395 the warm season of 2014.

Figure 5: Statistical error indices of the original and blended multi-SPE (i.e., PERCDR, 3B42V7, CMORPH, and IMERG) for 10 random tests during the warm season of 2014: (a) RMSE, (b) NMAE and (c) CC.

Figure 6: The Box-Whisker plots of improvement ratios of statistics for the blended multi-SPE compared to the original PERCDR, 3B42V7, CMORPH, and IMERG for 10 random tests during the warm season of 2014: (a) RMSE, (b) NMAE
400 and (c) CC.

Figure 7: Spatial patterns of the daily mean precipitation derived from the original multi-SPE during the warm season of 2014: (a) PERCDR, (b) 3B42V7, (c) CMORPH, and (d) IMERG.



- Figure 8:** Spatial patterns of the blended multi-SPE in terms of (a) median, (b) standard deviation, (c) 5% and (d) 95% quantiles for daily mean precipitation during the warm season of 2014.
- 405 **Figure 9:** (a) Spatial pattern of gauge measurements during a heavy rainfall case on Sep 22, 2014 over the NETP, where the site IDs 56171, 56152 and 56182 report the top three daily rainfall amounts of 30.4 mm, 24.6 mm and 23.1 mm, respectively; (b) the corresponding Box-Whisker plots of relative weights of the bias-adjusted multi-SPE (i.e., PERCDR, 3B42V7, CMORPH and IMERG) in the stage 2 process.
- Figure 10:** The PDF curves of blended samples and the corresponding median value at three gauge sites during a heavy
- 410 rainfall case on Sep 22, 2014: (a) ID 56171, (b) ID 56152, and (c) ID 56182. The individual SPE including PERCDR, 3B42V7, CMORPH, and IMERG as well as gauge based measurement at each pixel are also indicated in the figure.



415

Table 1: Basic information of multi-SPE used in this study.

Short name	Full name and details	Temporal resolution	Spatial resolution	Input data	Retrieval algorithm	References
PERCDR	Precipitation Estimation from Remotely Sensed Information using Artificial Neural Networks (PERSIANN) Climate Data Record (CDR)	Daily	0.25°	2014.5-2014.9	Adaptive artificial neural network	<i>Ashouri et al., 2015</i>
3B42V7	TRMM Multi-satellite Precipitation Analysis (TMPA) 3B42 Version 7	3 hourly	0.25°	2014.5-2014.9	GPCC monthly gauge observation to correct this bias of 3B42RT	<i>Huffman et al., 2007</i>
CMORPH	Climate Prediction Center (CPC) MORPHing technique for bias-corrected product	3 hourly	0.25°	2014.5-2014.9	Morphing technique	<i>Joyce et al., 2004</i>
IMERG	Integrated Multi-satellite Retrievals for the Global Precipitation Measurement (GPM) mission	0.5 hourly	0.10°	2014.5-2014.9	2014 version of the Goddard profiling algorithm (GPROF2014)	<i>Huffman et al., 2018</i>



420 2014.

Table 2: Summary of statistical error indices (i.e., RMSE, NMAE, and CC) in terms of the original, bias-adjusted, and blended multi-SPE (i.e., PERCDR, 3B42V7, CMORPH, and IMERG) at the validated sites of NETP in the warm season of

SPE	Type	RMSE (mm/d)	NMAE (%)	CC
PERCDR	Original	7.36	74.6	0.42
	Adjusted	5.02	58.7	0.42
3B42V7	Original	8.07	83.5	0.40
	Adjusted	5.06	57.5	0.41
CMORPH	Original	6.59	67.5	0.49
	Adjusted	4.81	54.6	0.50
IMERG	Original	7.18	63.2	0.57
	Adjusted	4.56	50.9	0.57
Blended multi-SPE		4.34	49.2	0.61



425 NETP.

Table 3: Summary of the mean values of statistics including RMSE, NMAE and CC in terms of the original and blended multi-SPE (i.e., PERCDR, 3B42V7, CMORPH, and IMERG) at 10 random verified tests in the warm season of 2014 over the

	RMSE (mm/d)	NMAE (%)	CC
PERCDR	7.72	78.5	0.38
3B42V7	7.57	78.9	0.43
CMORPH	6.21	66.3	0.51
IMERG	7.37	70.0	0.57
Blended	4.98	54.9	0.60



430 **Table 4:** Summary of the mean improvement ratios of statistics including RMSE, NMAE and CC in terms of the blended multi-SPE as compared to the original PERCDR, 3B42V7, CMORPH, and IMERG at 10 random verified tests in the warm season of 2014 over the NETP.

	Index	PERCDR	3B42V7	CMORPH	IMERG
Improvement Ratio (%)	RMSE	35.1	33.7	19.6	32.1
	NMAE	29.8	30.1	17.0	21.3
	CC	61.3	38.2	17.5	4.3



Table 5: Summary of statistical error indices (i.e., RMSE, NMAE, and CC) in terms of the original and blended multi-SPE (i.e., PERCDR, 3B42V7, CMORPH, and IMERG) during a heavy rainfall event over the NETP on Sep 22, 2014.

Multi-SPE	RMSE (mm/d)	NMAE (%)	CC
PERCDR	6.28	40.6	0.82
3B42V7	10.12	59.5	0.69
CMORPH	6.80	45.6	0.73
IMERG	10.48	53.3	0.81
Blended	4.13	27.4	0.85

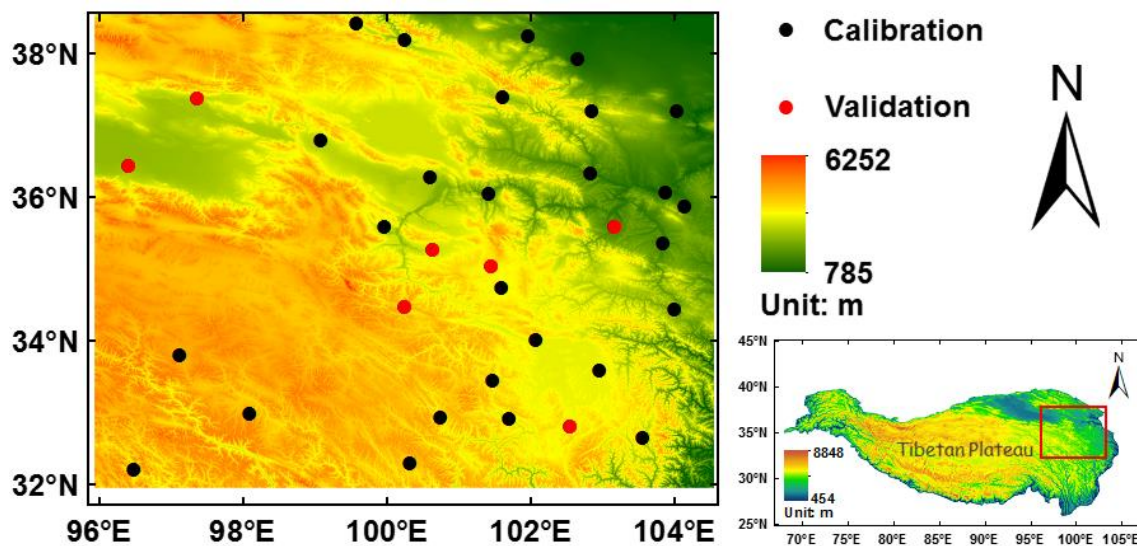


Figure 1: Overview of the topography and gauge observation network used in the study, where 27 gauges (black dots) are used for training and 7 (red dots) are used for independent verification.

440

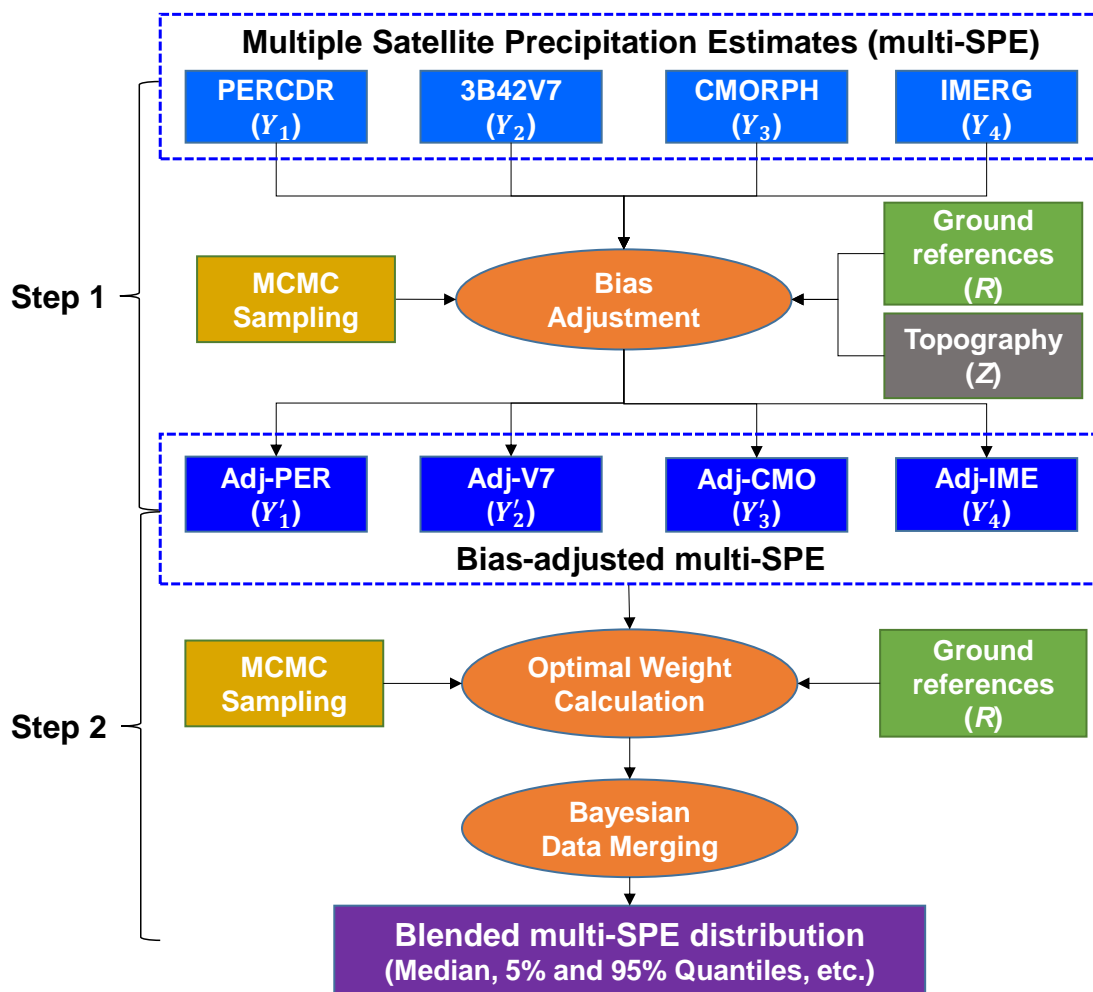
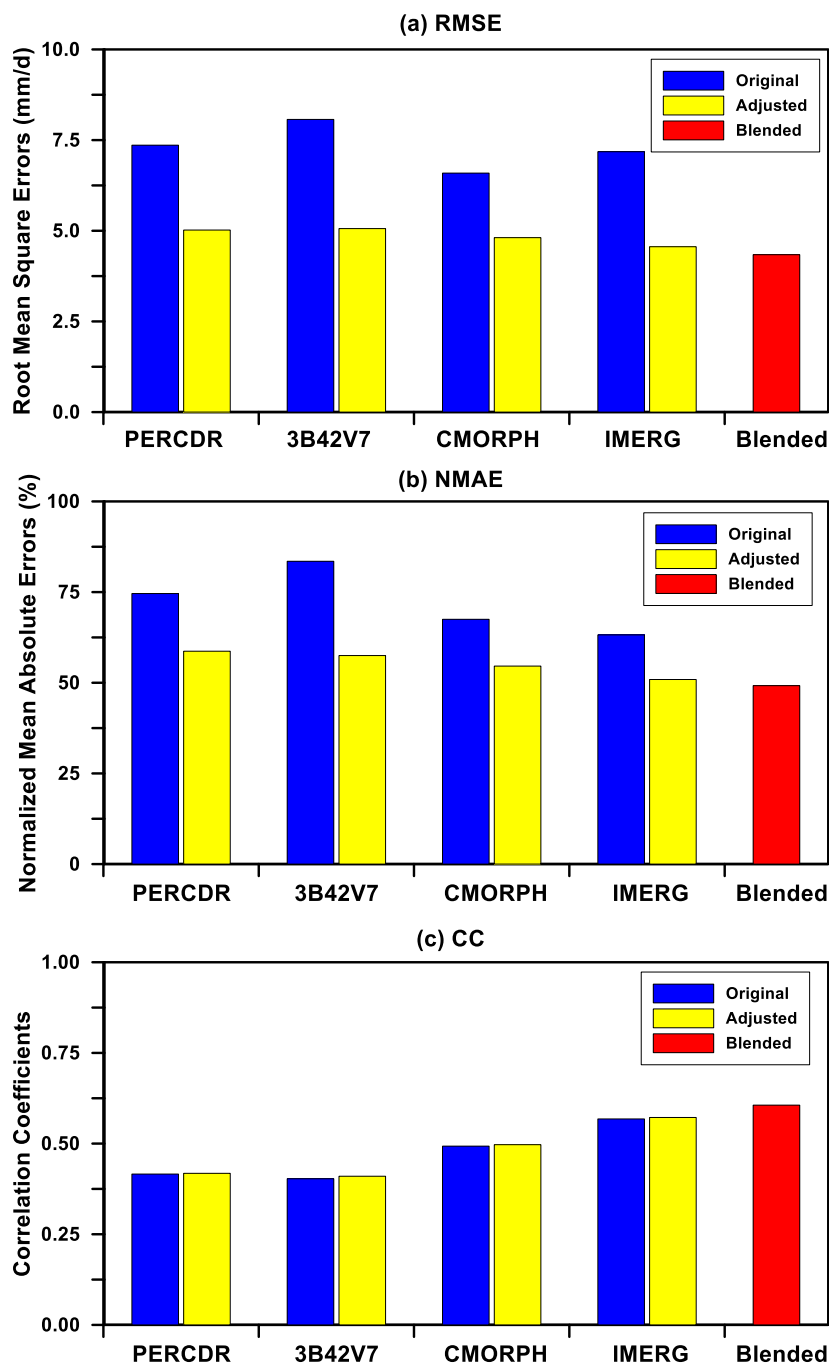


Figure 2: The diagram of the proposed two-step SPE blending algorithm.



445 **Figure 3:** Intercomparison of statistical error indices for the original, bias-adjusted, and blended multi-SPE at the validated sites during the warm season of 2014: (a) RMSE, (b) NMAE, and (c) CC.

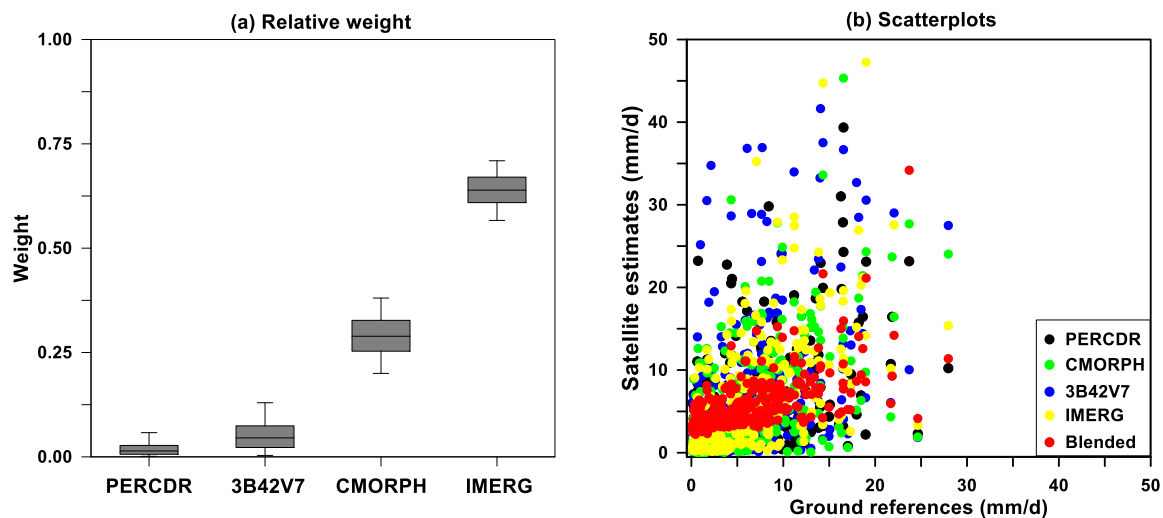


Figure 4: (a) The Box-Whisker plots of relative weights of the bias-adjusted multi-SPE (i.e., PERCDR, 3B42V7, CMORPH and IMERG) in the stage 2 process; (b) intercomparison of the original and blended multi-SPE at the validated sites during the warm season of 2014.

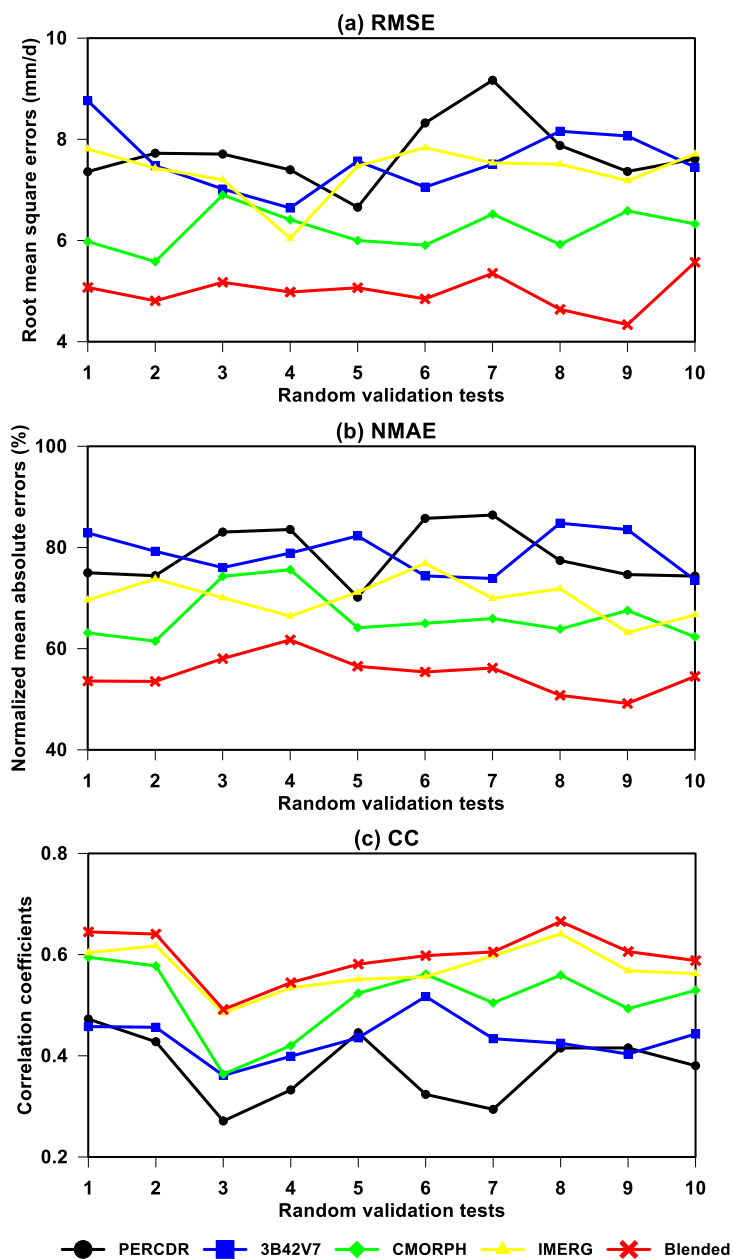


Figure 5: Statistical error indices of the original and blended multi-SPE (i.e., PERCDR, 3B42V7, CMORPH, and IMERG) for 10 random tests during the warm season of 2014: (a) RMSE, (b) NMAE and (c) CC.

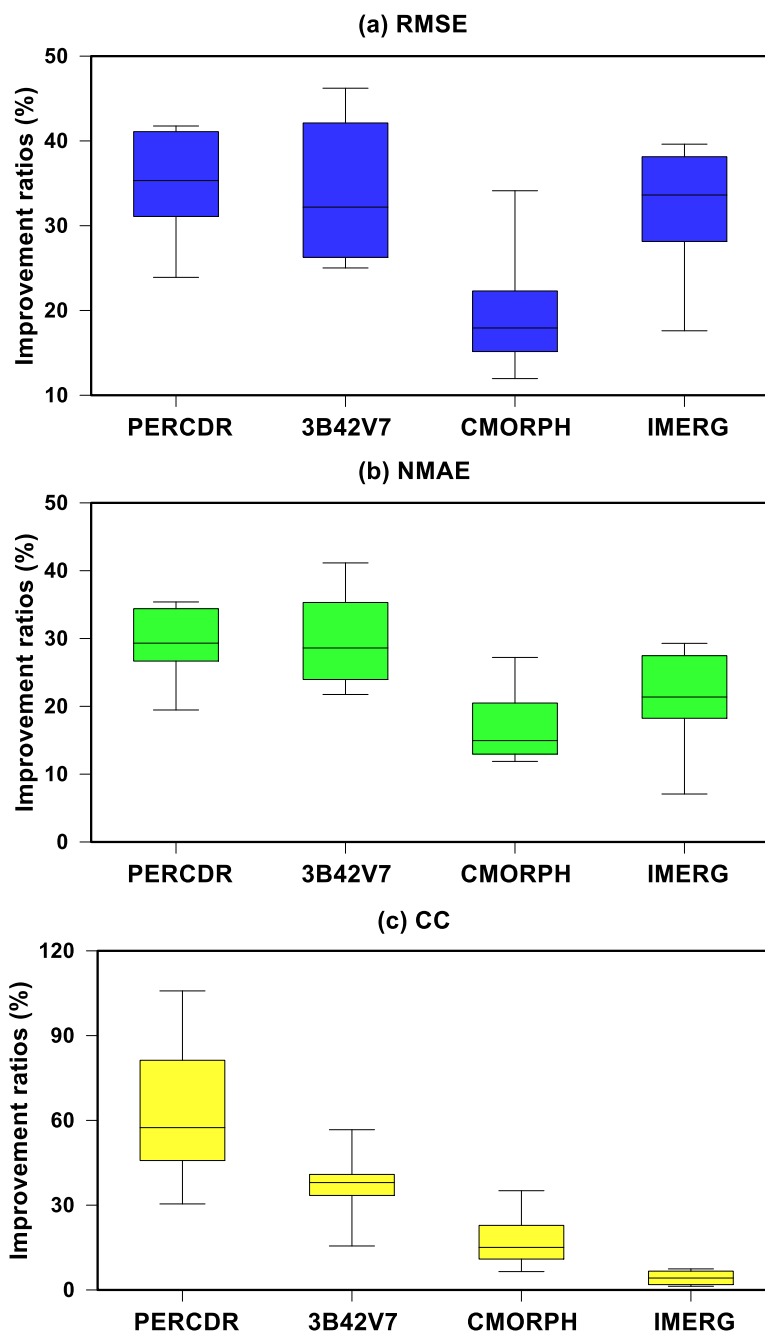


Figure 6: The Box-Whisker plots of improvement ratios of statistics for the blended multi-SPE compared to the original PERCDR, 3B42V7, CMORPH, and IMERG for 10 random tests during the warm season of 2014: (a) RMSE, (b) NMAE and

460 (c) CC.

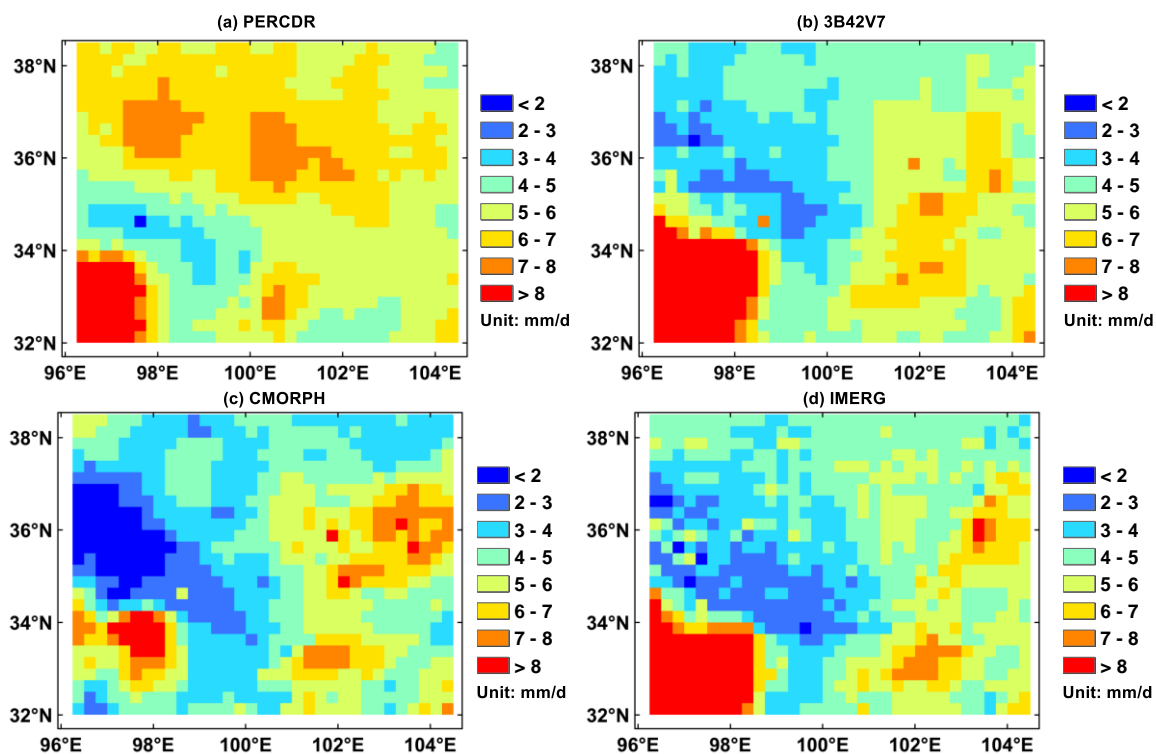


Figure 7: Spatial patterns of the daily mean precipitation derived from the original multi-SPE during the warm season of 2014: (a) PERCDR, (b) 3B42V7, (c) CMORPH, and (d) IMERG.

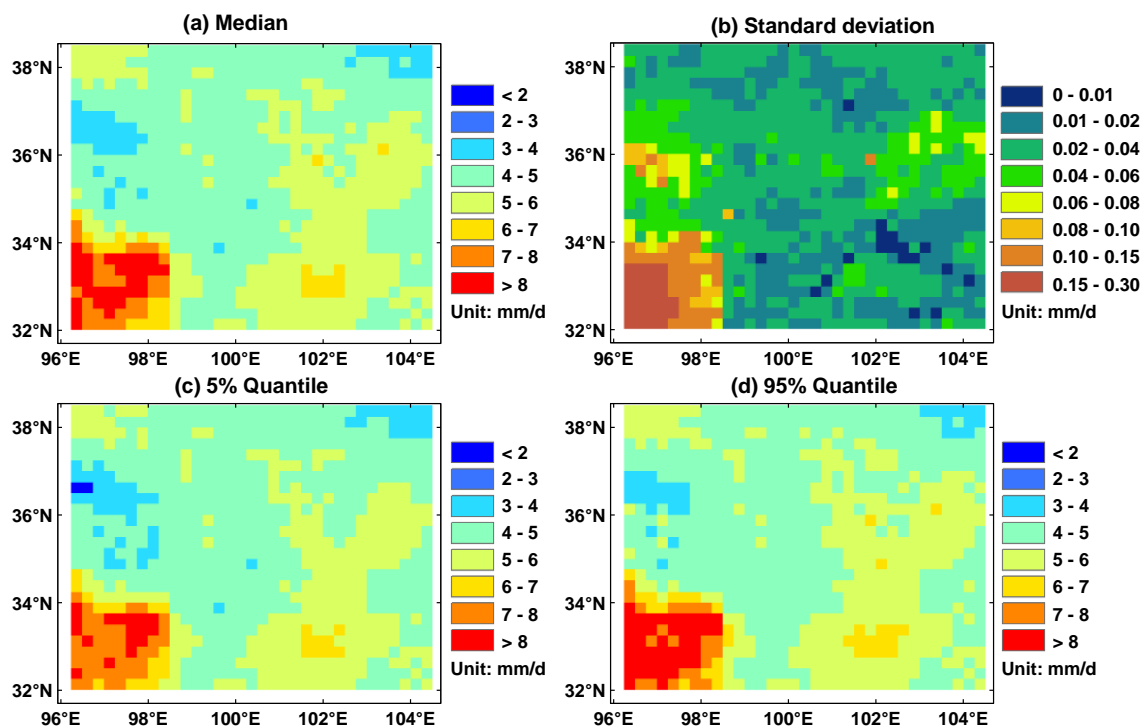
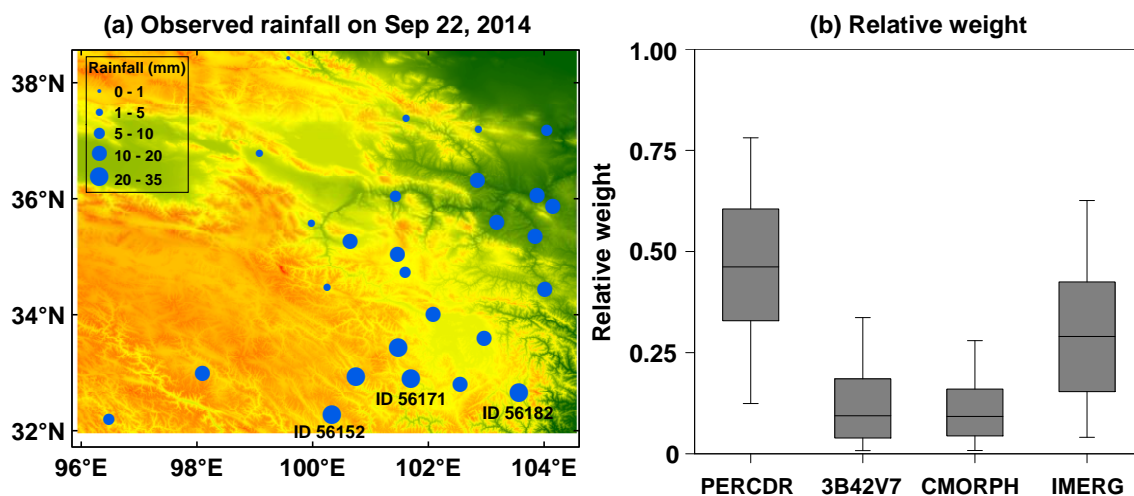


Figure 8: Spatial patterns of the blended multi-SPE in terms of (a) median, (b) standard deviation, (c) 5% and (d) 95% quantiles for daily mean precipitation during the warm season of 2014.



470

Figure 9: (a) Spatial pattern of gauge measurements during a heavy rainfall case on Sep 22, 2014 over the NETP, where the site IDs 56171, 56152 and 56182 report the top three daily rainfall amounts of 30.4 mm, 24.6 mm and 23.1 mm, respectively; (b) the corresponding Box-Whisker plots of relative weights of the bias-adjusted multi-SPE (i.e., PERCDR, 3B42V7, CMORPH and IMERG) in the stage 2 process.

475

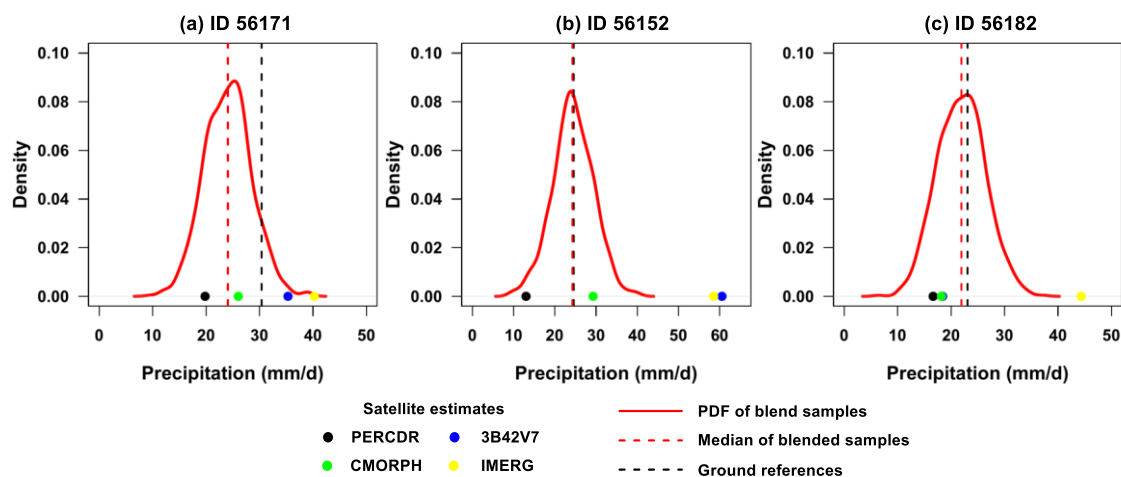


Figure 10: The PDF curves of blended samples and the corresponding median value at three gauge sites during a heavy rainfall case on Sep 22, 2014: (a) ID 56171, (b) ID 56152, and (c) ID 56182. The individual SPE including PERCDR, 3B42V7, CMORPH, and IMERG as well as gauge based measurement at each pixel are also indicated in the figure.